Space Vector Modulation Current Control of a Three-Phase PV Grid-Connected Inverter

A. Althobaiti, M. Armstrong, and M. A. Elgendy

School of Electrical and Electronic Engineering,
Newcastle University, NE1 7RU, United Kingdom
ahmed.althobaiti@ncl.ac.uk; matthew.armstrong@ncl.ac.uk; mohammed.elgendy@ncl.ac.uk

Abstract— **In recent years, there has been a rapid increase in the number of photovoltaic (PV) three phase inverter systems being to grid connected. Keeping the highly quality waveform and low harmonic distortion of the current waveform during abnormal condition is one of the most challenging. To achieve this target, a current control technique is carefully considered. This paper present a simple method to compensate the reactive power to the grid connected inverter to deal with abnormal grid condition. The control system using space vector modulation (SVM) with the more recently adopted Proportional Resonant controller (PR). The proposed technique will show an effective method for grid-connected application. Simulation results will demonstrate the effectiveness of the proposed technique.**

Keywords— Proportinal Resonant; abnormal grid conditions, Grid-connected Inverter; LCL filter.

I. INTRODUCTION

Distributed Generation (DG) is now widely employed in based on energy storage and renewable energy sources such as wind power, solar cells power and hydropower which lead to a reduction in carbon dioxide emissions[1]. A three-phase grid connected inverter is used to interface the photovoltaic (PV) panels which is transform a DC voltage into the appropriate AC voltage for the utility grid. In fact, there are two main types of connection of PV panels to the utility gird as shown in Fig.1. The first method is a single stage where the PV panels are connected in series or parallel to achieve certain voltage and current levels due to the low input voltage provided from the PV system. The second method is a dual or double stages converter system which has. a DC-DC converter which can be used in this application to boost the voltage to the higher desired values with maximum power point tracking (MPPT) to work at the highest efficiency point and acceptable level of different kinds of the inverters. The second stage converts the DC value to the three phase AC values via a three-phase inverter.

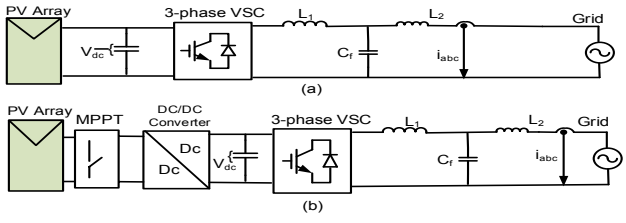

Fig.1 Diagrams of grid connected three-phase inverters. (a) single stage, (b) double stage

The inverter and the associated control system are at the core of the energy conversion process and their operation is essential to inject high power quality, low harmonic distortion, current to the grid [2]. For this reason international harmonic and power quality recommendations, such as IEEE Standard 519 and 1547, are often in place to limit the any harmonic components added into the utility grid [3]. Typically, 5% current total harmonic distortion (THD) limit is imposed.

Numerous inverter current control techniques have been proposed to achieve improved power quality waveforms. The proportional-integral controller (PI controller) is perhaps the best understood and commonly applied control strategy. In three phase systems, the d-q rotating synchronous reference frame (SRF) approach, based on classic Park transformations, is often applied [4]. As a consequence of the shortcomings of the PI controller such as steady state output error when tracking sinusoidal reference signals [5], alternative control solutions have been presented. Of these, the Proportional Resonant (PR) controller has become a popular strategy in renewable energy applications. For example, in [6], the PR controller is successfully employed in the stationary reference frame of a three phase grid connected system. Significantly, the reported advantages of the PR controller include the capability to remove steady state errors when tracking AC signals by generating an infinite gain at a known resonant frequency of the controlled signal [7], and a highly attenuated gain at other frequencies, such as the harmonic frequencies. Furthermore, the Park transformation is not necessary, and there is less cross coupling of the control axis, hence de-coupling strategies are not required [8]. As a result, in grid connected applications, significant reduction in the harmonic content of the controlled current is possible. Additional elimination of the harmonic content can be achieved by implementing Harmonic Compensation (HC) terms in parallel with the main control effort [9].

However, a sudden drop in the voltage could further increase the error between the reference signal and the controlled signal causing considerable deviation from its nominal value. The performance of the conventional PR controller will not keep up with the increase in the error which weakens the controller performance. To overcome this issue, this paper presents an improvement in current control using a novel adaptive PR controller. It demonstrates and compares the performance of the adaptive PR controller during normal and abnormal grid voltage conditions. The proposed control technique is capable of providing low total harmonic distortion (THD) of the

injected current even during the occurrence of abnormal grid conditions. The proposed method also achieves lower overshoot, settling time as well as steady-state error.

A simple method is presented in this paper to decompose the voltage and the current into their positive and negative sequence components based on adaptive delayed filter with one-quarter period delay. The performance of the adaptive control strategy is verified by simulation and experimental results.

The three-phase grid-connected inverter is modeled and controlled using adaptive PR controller strategy based on the stationary reference frame (SRF) point of view with space vector modulation technique (SVM). As a result, a phase locked loop (PLL) is used here in this control to detect the transformation angle and enhance the synchronization of the inverter output current with the grid voltages achieved. Two adaptive PR current controllers together with harmonic compensators are applied in the current controller. Due to the absence of the connection between decoupled active and reactive components, as a result excellent dynamic response can be succeeded.

II. PV MODULE

A photovoltaic (PV) cell is the source and the core of the power conversion system. The concept of the PV cell came from the simple P-N junction semiconductor. Light crosses the junction where the current flows in both directions and produces electrical load. The PV cell circuit model contains of an ideal current source in parallel with an ideal diode. Thus, the diode determines the equivalent circuit I-V characteristics of solar cell as shown in the Fig.2, where I_{ph} is the photo current source and is dependent on the solar irradiance and ambient temperature, and I_j is the shunt current through the diode.

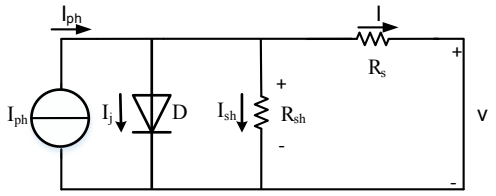

Fig.2 Equivalent circuit I-V characteristics of solar cell

According to Kirchhoff's current law, the output current is given by [10]:

$$I = I_{ph} - I_j \tag{1}$$

The current voltage relationship of the PV cell is given by the I-V equation:

$$I = I_{ph} - I_o \left\{\exp\left(\frac{q.V}{AKT}\right) - 1\right\} - \frac{V}{R_{sh}} \tag{2}$$

where, I_{ph} is the photon current and I_j is the diode current. I_{sh} is the shunt current, D is the parallel diode. R_{sh} is the shunt resistance and R_s is the series resistance. I_o is the reverse saturation current of the diode, q is the electron charge $q = 1.6 * 10^{-19}\ C$, A is the current fitting factor, K is Boltzmann's constant $A = 1.381 * 10^{-23}\ J/K$ and T is the junction temperature (K). By assuming the R_{sh}=∞ the previous equation can be reduced to:

$$I = I_{ph} - I_o \left\{\exp\left(\frac{q.V}{AKT}\right) - 1\right\} - 1 \tag{3}$$

The characteristics of the PV panels between (I-V) and (P-V) are non-linear. Therefore, a Maximum Power Point Tracking (MPPTT) algorithm is essential. Due to it is simplicity, the most widely used MPPT technique is Perturb & Observe (P&O) method [11]. Thus, the output voltage is the reference DC either to the DC-AC inverter as a single stage or to the DC-DC dual stage.

III. LCL FILTER MATHEMTCAL MODEL

A three-phase grid connected inverter with a third order LCL filter is shown in Fig.3. The LCL filters is used to increase the power quality of the output current compared to lower order L and LC filters [12].

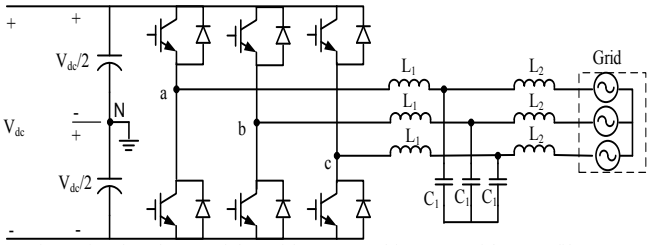

Fig.3 Simple scheme of the grid-connected inverter with LCL-filter

The differential equation representing of the LCL filter can be found from the equivalent circuit of the single-phase in Fig 3. Here, the filter is defined by the inverter-side inductor L_1, filter capacitor C_1, grid-side inductor L_2, and the resistive elements represent the ohmic losses in the passive components.

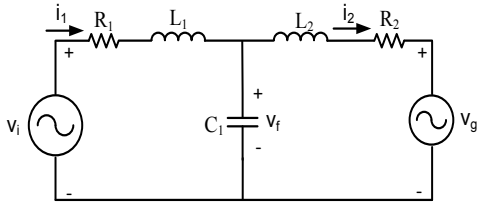

Fig.4 single-phase equivalent circuit of the LCL filter

Since SVM is used in this system, the LCL filter is designed in the SRF frame (αβ) using space vectors to make it easier and more convenient. By applying Kirchhoff's current and voltage laws, the following equations can be used to represent the voltages and currents within the circuit of fig.4 [13].

$$\bar{v}_{i(\alpha,\beta)} = \bar{S}_{(\alpha,\beta)} \frac{v_{dc}}{2} \tag{4}$$

$$\bar{v}_{i(\alpha,\beta)} - \bar{v}_{f(\alpha,\beta)} = R_1 \bar{\imath}_{1(\alpha,\beta)} + L_1 \frac{d\bar{\imath}_{1(\alpha,\beta)}}{dt} \tag{5}$$

$$\bar{v}_{f(\alpha,\beta)} - \bar{v}_{g(\alpha,\beta)} = R_2 \bar{\imath}_{2(\alpha,\beta)} + L_2 \frac{d\bar{\imath}_{2(\alpha,\beta)}}{dt} \tag{6}$$

$$\bar{\imath}_{cf(\alpha,\beta)} = \bar{\imath}_{1(\alpha,\beta)} - \bar{\imath}_{2(\alpha,\beta)} \tag{7}$$

where; $\bar{v}_{i(\alpha,\beta)}$ is the output voltage vector of the inverter, v_{dc} is the dc voltage, $\bar{S}_{(\alpha,\beta)}$ is the space vector switching, $\bar{v}_{f(\alpha,\beta)}$ is the voltage vector of the capacitor, $\bar{v}_{g(\alpha,\beta)}$ is the voltage vector of the grid side, R_1 is the inverter resistance, $R_2$is the grid resistance, L_1 is the inverter side inductor, $L_2$is the grid side inductor; $\bar{\imath}_{cf(\alpha,\beta)}$, $\bar{\imath}_{1(\alpha,\beta)}$ and $\bar{\imath}_{2(\alpha,\beta)}$ are the current vectors of the LCL filter. The resonant frequency in Fig.4 can be calculated using:

$$f_{ref} = \frac{1}{2\pi}\sqrt{\frac{L_1+L_2}{L_1 L_1 C}} \quad (8)$$

Note, the resonant frequency f_{res} should be not less than 10 times of the line frequency f_n , and lower than half of the PWM switching frequency f_{sw} to avoid resonance issue in the grid-connected application [14].

IV. Space Vector Modulation

Space vector modulation (SVM) is a modulation technique that become popular in the control and widely applied in three-phase grid-connected inverter. SVM is flattering best Pulse Width Modulation (PWM) technique due to the many features of SVM such as SVM can provide 15% higher output voltage than the sinusoidal PWM.

SVM can be designed as a single unit. This unit has eight switching levels; each switching state describes the voltage space vector as a point in 2-dimensional complex vector mapping in $\alpha\beta$. Figure 1-8 shows the vector hexagonal shape of the SVM. The shape is divided in six non-zero switching sectors from U_1 to $U_6$where U_0 and U_7 are lining in the origin position of the hexagon.

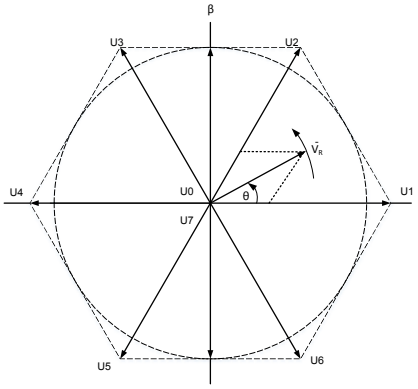

Fig. 5 Space Vector hexogen

In SVM, the three phase reference voltages U_a , U_b and U_c are converted to complex two phase orthognal $\alpha\beta$ plane using a Clarks transformation as shown in the following matrix:

$$\overline{V_R} = \begin{bmatrix} U_\alpha \\ U_\beta \end{bmatrix} = \begin{bmatrix} 2/3 & -1/3 & -1/3 \\ 0 & 1/\sqrt{3} & -1/\sqrt{3} \end{bmatrix} \begin{bmatrix} U_a \\ U_b \\ U_c \end{bmatrix} \quad (9)$$

V. Control Scheme

In this work, the applied control system is a cascaded system in which the outer voltage control loop controls the inner current control loop. The block diagram of the PR current control scheme is presented in Fig. 6. The voltage control loop comprises of two PI regulators; one for the dc link voltage control and the other for the grid voltage control. The measured dc voltage is compared with the reference dc voltage $v_{dc(ref)}$ in the dc voltage control.

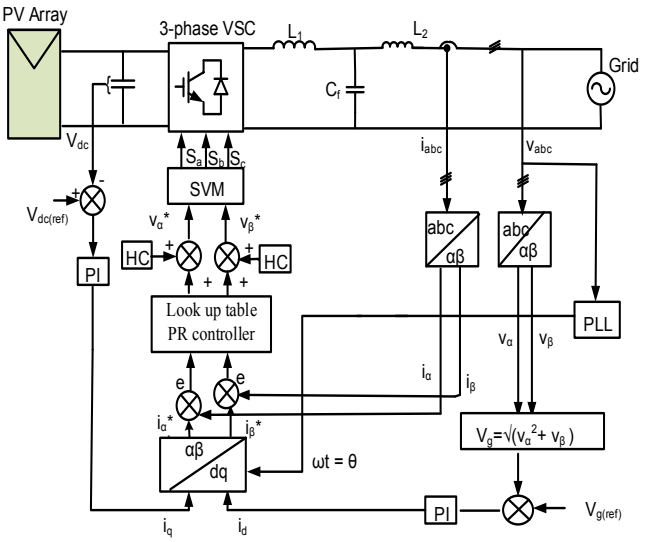

Fig.6 Adaptive PR controller in stationary reference control

Here, it is essential to convert the three phase alternating *abc* voltage and current waveforms into two phase $\alpha\beta$ components using a Clarke transformation, as shown in the following equations [15]. [15, 16] .

$$\begin{bmatrix} v_{g(\alpha)} \\ v_{g(\beta)} \end{bmatrix} = \frac{2}{3}\begin{bmatrix} 1 & -\frac{1}{2} & -\frac{1}{2} \\ 0 & \frac{\sqrt{3}}{2} & -\frac{\sqrt{3}}{2} \end{bmatrix} \begin{bmatrix} v_{g(a)} \\ v_{g(b)} \\ v_{g(c)} \end{bmatrix} \quad (10)$$

$$\begin{bmatrix} i_{(\alpha)} \\ i_{(\beta)} \end{bmatrix} = \frac{2}{3}\begin{bmatrix} 1 & -\frac{1}{2} & -\frac{1}{2} \\ 0 & \frac{\sqrt{3}}{2} & -\frac{\sqrt{3}}{2} \end{bmatrix} \begin{bmatrix} v_{g(a)} \\ v_{g(b)} \\ v_{g(c)} \end{bmatrix} \quad (11)$$

In this control scheme, the PLL is used to synchronize the output current of the converter to the grid voltage. As such, it is essential in controlling the phase angle and frequency of the system. Fig.7 displays the PLL block diagram.

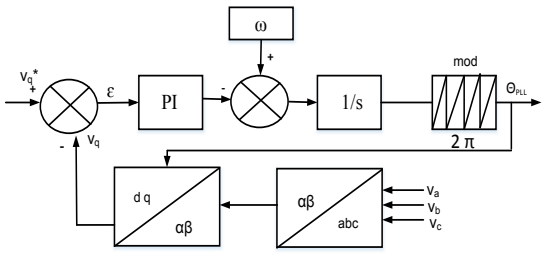

Fig.7 Block diagram of three phase PLL

The measured voltage is converted to the synchronous reference frame, and v_q (the q-component) is compared with the reference v_q^* which is equal to zero and controlled by a PI controller. The nominal grid frequency ω is added to the output of the PI controller, and the the grid voltage angle θ can be obtained by integrated the sum of the PLL.

The grid voltage amplitude is compared with the reference grid voltage amplitude $|v_{g(ref)}|$ in the grid voltage controller.

The grid voltage amplitude is calculated in the stationary reference frame using the equation below.

$$|V_{PCC}| = \sqrt{v_{g(\alpha)}{}^2 + v_{g(\beta)}{}^2} \tag{12}$$

The error between the measured grid voltage and the reference grid voltage is fed to a PI controller whose transfer function is given below.

$$G_{pi}(s) = k_p + \frac{k_i}{s} \tag{13}$$

As such, the outputs of the voltage controllers serve as the current references in the d-q reference frame. To obtain the current references in the stationary reference frame, in which the PR controller is implemented, the d-q current references are transformed using the inverse Park transformation is:

$$\begin{bmatrix} i_d^* \\ i_q^* \end{bmatrix} = \begin{bmatrix} \cos\theta & -\sin\theta \\ \sin\theta & \cos\theta \end{bmatrix} \begin{bmatrix} i_\alpha^* \\ i_\beta^* \end{bmatrix} \tag{14}$$

where; θ is the grid voltage angle obtained from the PLL.

The PR controller transfer function is:

$$G_{PR}(s) = K_p + K_i \frac{s}{(s^2 + \omega^2)} \tag{15}$$

Where, ω is the resonant (line) frequency. Because of the high observable gain at fundamental frequency, ω, steady state error can be typically removed via PR controller. A chart diagram of the PR control scheme is presented in Fig.8.

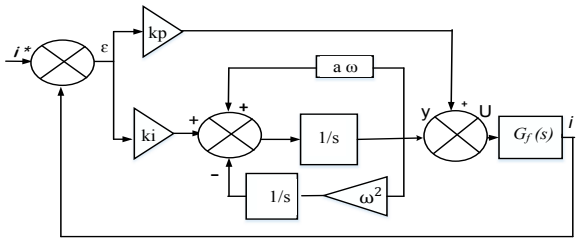

Fig.8 Control Diagram of PR controller implementation

However, to avoid the problem of obtaining infinite gain at the resonant frequency, a non-ideal PR controller which is given in the following equation can instead be used:

$$G_{PR}(s) = K_p + K_i \frac{2\omega_c s}{(s^2 + 2\omega_c s + \omega_0{}^2)} \tag{15}$$

where; ω_c is the bandwidth of the cutoff frequency and $\omega_c \gg \omega_0$. Fig.9 illustrates the bode diagram for both ideal PR and non-ideal PR controllers. It clearly shows that the non-ideal PR controller has less gain in the narrow frequency all over the resonance frequency compare with ideal one.

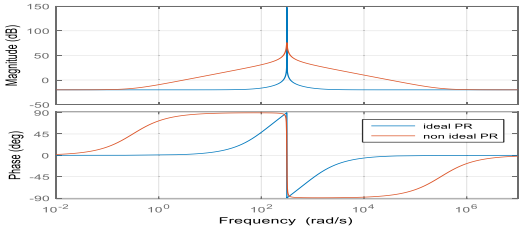

Fig.9 The bode plots of PR controller ideal and non-ideal controllers

The PR controller can be readily implemented on a digital signal processor (DSP) after conversion to discrete form. The generalized discrete equivalent of the PR controller, converted to the z domain using backward Euler method. The difference equation, which is implemented in C-code in the DSP is given by the equation below:

$$y1 = k_p$$

$$y_2(k+2) = 2y_2(k+2) - \left(1 + \omega^2 T_s{}^2\right)y_2(k) + k_i T_s\,[x(k+1) - x(k)] \tag{13}$$

Where, y_1, y_2 are output of controller and ω is the resonant frequency, T_s is the sample time. In order to reach higher performance level of the control system, a Harmonic Compensator (HC) is implemented in parallel with the main PR control scheme. Note that the HC does not impact upon the efficiency of the basic PR controller. However, it has a major effect on the harmonic frequency to which the compensator is tuned [8]. In grid connected applications, it is common to implement HC terms in parallel with the basic PR controller to target low order harmonics (5^{th}, 7^{th}); these are well recognised as being problematic. The HC can be implemented by following the equation below:

$$G_{HC}(s) = \sum_{h=5,7} \frac{2\ K_{ih}\ s}{s^2 + (\omega h)^2} \tag{14}$$

Where, K_{ih} is the individual resonant gain, h is the harmonic order.

VI. Proposed ControlStrategy

In this study, the adaptive PR controller strategy is used to adapt the static gains of the proportional part and the integral part of the PR controllers. The on-line adaptation is based on a look-up table which is used to update the controller parameters using the following equations:

$$k_p(k+1) = k_p(k) + \Delta k_p(k) \tag{21}$$

$$k_i(k+1) = k_i(k) + \Delta k_i(k) \tag{22}$$

When the sudden error is increased beyond the maximum allowed variation of 5%, the adaptive controller will auto tune both the kp and the ki of the PR controller. One potential cause of such an increase in error is voltage sag. A voltage sag is a temporary reduction in the RMS voltage between 90% to 10% and the duration time from half cycle up to a few seconds) [17].

VII. Result and Discussion

A. Simulation Reasult

The system in Fig.6 is simulated in MATLAB®. A 100kW system is simulated, and the nominal operating parameters of the simulation are identified in Table 1 below.

TABLE 1. Simulation parameter of the system

Parameter	Value
Power Rating	100kW
Voltage grid (line to line)	415 V
Inverter side inductance	5.0 m H
Grid side inductance	3.0 m H

DC voltage	760 V
DC capacitor	2000 µF
Sampling frequency & Switching frequency	10 kHz
Filter capacitor	92 µF

Fig. 10 shows the simulation results of the three phase voltage and current. Fig.10 (a) shows the three phase voltage waveform. It can be seen that the voltage drops when a voltage sags happens in the system at 0.1 sec until 0.15 sec. Fig.10 (b) shows three phase current waveform. It is clear that the current has increased when the sudden voltage occur at 0.1 sec in order to balance the active power transfer from the PV source. Fig.11 (a) and fig.11 (b) show the stationary reference frame alpha and beta current waveform respectively. The measured current following the reference current which they point out that the adaptive PR controller works effectively when there is change in the grid conditions.

However, in the case of unbalanced voltage sag the adaptive PR controller achieves better dynamic response. Fig.12 (a) and Fig.12 (b) shows the three phase voltage and current waveform respectively; note the reduction in the overshoot characteristics and the recovery time to achieve steady state. It is clear that the adaptive controller can better compensate the unbalanced current. It can be shown that this is due to the adaptive controllers improved ability to control the positive and negative sequence components.

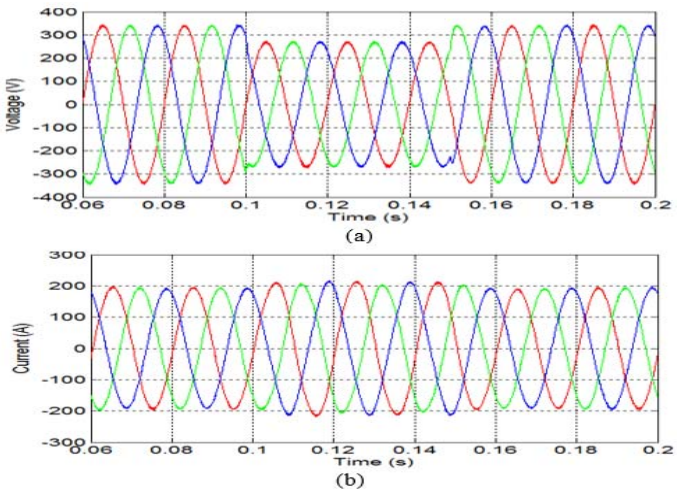

Fig. 10 Simulation result waveforms. (a) Three phase voltage waveform. (b)Three phase current waveform.

A. Experimintal Reasult

To validate the control technique presented above, experimental results are obtained using a small scale three phase laboratory prototype inverter connected to the grid. The control is implemented on a Texas instrument eZdspF28335 DSP. The nominal operating parameter are defined in table 2.

TABLE 2. Practical parameters of the system

Parameter	Value
Power rating	300W
Voltage grid [line to line]	35 V
Inverter side inductance	0.6 mH
Grid side inductance	0.175 mH
Dc-link voltage	50 V
Dc capacitor	1500 µF
Switching frequency & Sampling frequency	10 kHz
filter capacitor	20 µF

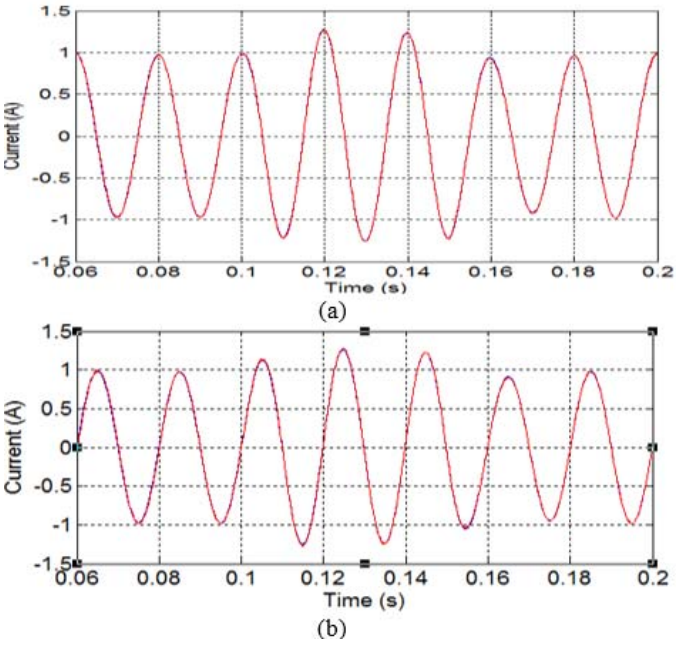

Fig. 11 Simulation result waveforms for adaptive PR controller. (a) i-alpha. (b) i-beta.

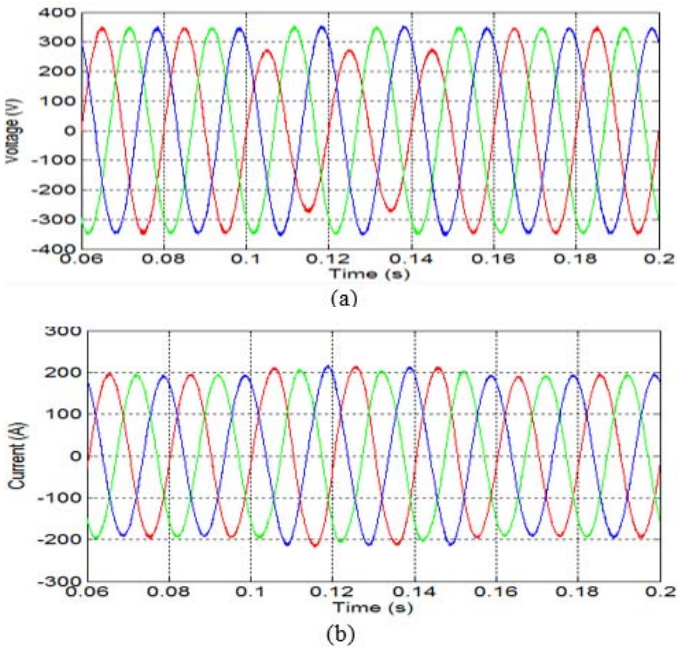

Fig.12 Simulation result waveforms under unbalanced grid condition. (a) Three phase voltage waveform. (b) Three phase current waveform.

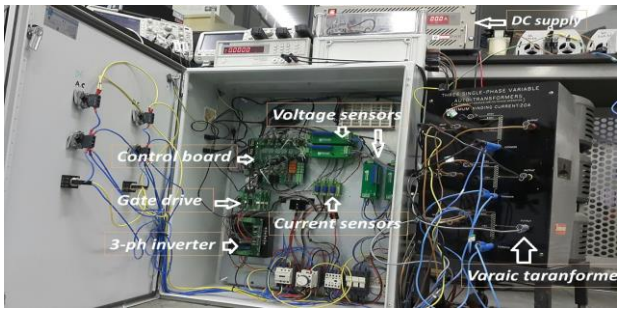

Fig. 13 Three phase inverter test rig

Fig.13 displays the experimental results of the inverter under stationary frame adaptive PR controller. Fig.14 (a) shows the three phase current waveform with the grid voltage. It can be observed that the current waveform is smooth and no oscillations appear in the waveform. Furthermore, the current THD is 3.82% which is less than the approved limits set by IEEE recommendations. Fig.14 (b) shows the reference alpha current and the measured alpha current; and the reference beta current and the measured beta current waveforms. It can be seen that the measured current accurately follows the reference current in both signals. In addition, Fig.14 (c) shows the three phase current when a step reference is applied. The waveforms show that the adaptive PR controller has a fast response with a small overshoot. The alpha and beta current waveform, when subjected to a step change, is shown in Fig. 14 (d).

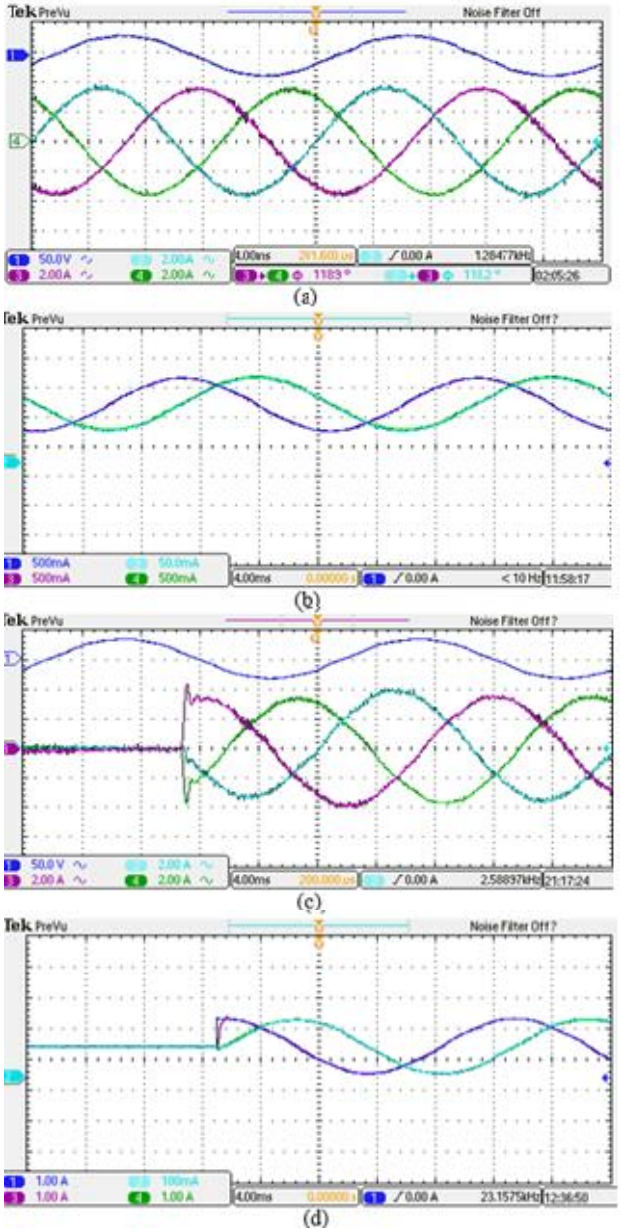

Fig. 14 Experimental result waveforms (a) the three phase current waveform (2A/div) lower waveform with the grid voltage (50V/div) upper waveform (b) the stationary reference frame (alpha) current waveform and the stationary reference frame (beta) current waveform. (c) the output of the three phase current with step response. (d) the stationary reference frame (alpha) current waveform and the stationary reference frame (beta) current waveform with step response

REFERENCES

[1] L. Wuhua and H. Xiangning, "Review of Nonisolated High-Step-Up DC/DC Converters in Photovoltaic Grid-Connected Applications," *Industrial Electronics, IEEE Transactions on,* vol. 58, pp. 1239-1250, 2011.

[2] B. Chenlei, R. Xinbo, W. Xuehua, L. Weiwei, P. Donghua, and W. Kailei, "Step-by-Step Controller Design for LCL-Type Grid-Connected Inverter with Capacitor–Current-Feedback Active-Damping," *Power Electronics, IEEE Transactions on,* vol. 29, pp. 1239-1253, 2014.

[3] "IEEE Standard for Interconnecting Distributed Resources With Electric Power Systems," *IEEE Std 1547-2003,* pp. 0_1-16, 2003.

[4] A. Nicastri and A. Nagliero, "Comparison and evaluation of the PLL techniques for the design of the grid-connected inverter systems," in *Industrial Electronics (ISIE), 2010 IEEE International Symposium on*, 2010, pp. 3865-3870.

[5] R. Teodorescu, F. Blaabjerg, U. Borup, and M. Liserre, "A new control structure for grid-connected LCL PV inverters with zero steady-state error and selective harmonic compensation," in *Applied Power Electronics Conference and Exposition, 2004. APEC '04. Nineteenth Annual IEEE*, 2004, pp. 580-586 Vol.1.

[6] S. Byeong-Mun, K. Youngroc, C. Hanju, and L. Hakju, "Current harmonic minimization of a grid-connected photovoltaic 500kW three-phase inverter using PR control," in *Energy Conversion Congress and Exposition (ECCE), 2011 IEEE*, 2011, pp. 1063-1068.

[7] M. Castilla, J. Miret, J. Matas, L. G. de Vicua, and J. M. Guerrero, "Linear Current Control Scheme With Series Resonant Harmonic Compensator for Single-Phase Grid-Connected Photovoltaic Inverters," *Industrial Electronics, IEEE Transactions on,* vol. 55, pp. 2724-2733, 2008.

[8] R. Teodorescu, F. Blaabjerg, M. Liserre, and P. C. Loh, "Proportional-resonant controllers and filters for grid-connected voltage-source converters," *Electric Power Applications, IEE Proceedings,* vol. 153, pp. 750-762, 2006.

[9] M. Liserre, R. Teodorescu, and F. Blaabjerg, "Multiple harmonics control for three-phase grid converter systems with the use of PI-RES current controller in a rotating frame," *Power Electronics, IEEE Transactions on,* vol. 21, pp. 836-841, 2006.

[10] R. Kadri, J. P. Gaubert, and G. Champenois, "An Improved Maximum Power Point Tracking for Photovoltaic Grid-Connected Inverter Based on Voltage-Oriented Control," *IEEE Trans, Ind. Electronic.,* vol. 58, pp. 66-75, 2011.

[11] M. A. Elgendy, B. Zahawi, and D. J. Atkinson, "Operating Characteristics of the P&O Algorithm at High Perturbation Frequencies for Standalone PV Systems," *IEEE Transactions on Energy Conversion,* vol. 30, pp. 189-198, 2015.

[12] M. Liserre, F. Blaabjerg, and S. Hansen, "Design and control of an LCL-filter-based three-phase active rectifier," *Industry Applications, IEEE Transactions on,* vol. 41, pp. 1281-1291, 2005.

[13] L. Bochuan and S. Byeong-Mun, "Modeling and analysis of an LCL filter for grid-connected inverters in wind power generation systems," in *Power and Energy Society General Meeting, 2011 IEEE*, 2011, pp. 1-6.

[14] R. Teodorescu and F. Blaabjerg, "Flexible control of small wind turbines with grid failure detection operating in stand-alone and grid-connected mode," *Power Electronics, IEEE Transactions on,* vol. 19, pp. 1323-1332, 2004.

[15] J. Svensson, "Synchronisation methods for grid-connected voltage source converters," *Generation, Transmission and Distribution, IEE Proceedings-,* vol. 148, pp. 229-235, 2001.

[16] J. Miret, M. Castilla, A. Camacho, Garci, x, V. a de*, et al.*, "Control Scheme for Photovoltaic Three-Phase Inverters to Minimize Peak Currents During Unbalanced Grid-Voltage Sags," *Power Electronics, IEEE Transactions on,* vol. 27, pp. 4262-4271, 2012.